UCRL-JC-135382
PREPRINT

Role of Interfacial Dislocations on Creep of a Fully Lamellar TiAl

T.G. Nieh
L.M. Hsiung

This paper was prepared for submittal to the
8th International Conference on Creep and Fracture of
Engineering Materials and Structures
Tsukuba City, Japan
November 1-5, 1999

August 16, 1999

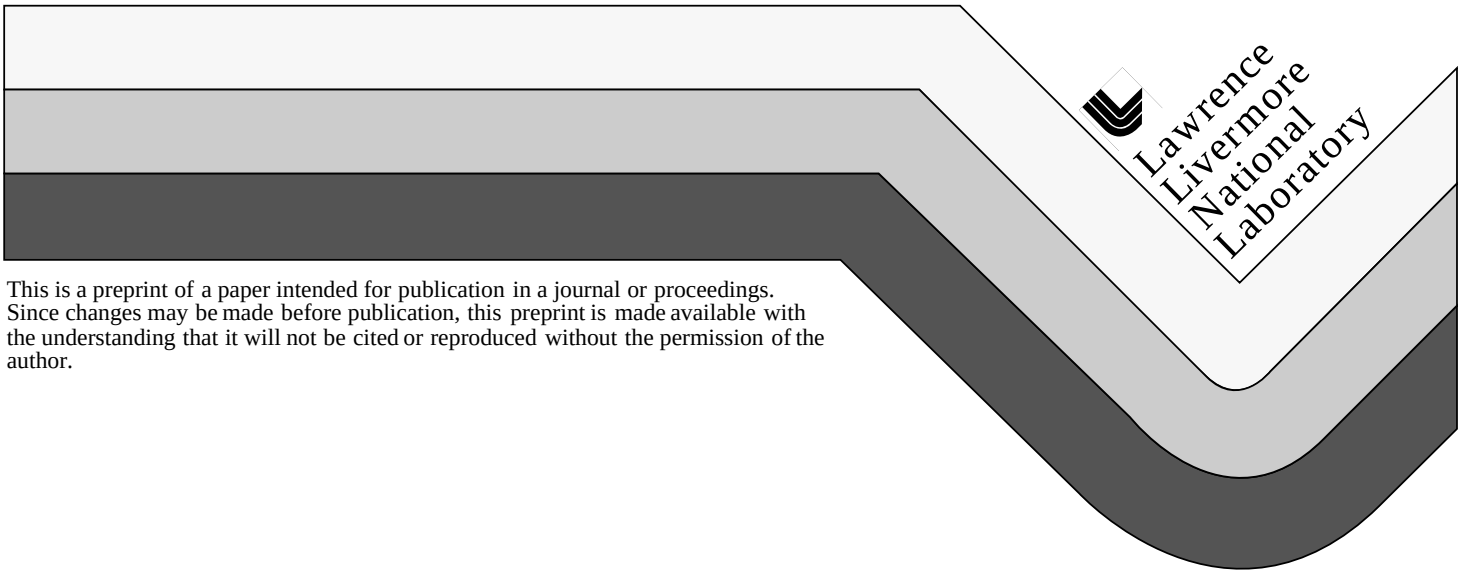

This is a preprint of a paper intended for publication in a journal or proceedings. Since changes may be made before publication, this preprint is made available with the understanding that it will not be cited or reproduced without the permission of the author.

DISCLAIMER

This document was prepared as an account of work sponsored by an agency of the United States Government. Neither the United States Government nor the University of California nor any of their employees, makes any warranty, express or implied, or assumes any legal liability or responsibility for the accuracy, completeness, or usefulness of any information, apparatus, product, or process disclosed, or represents that its use would not infringe privately owned rights. Reference herein to any specific commercial product, process, or service by trade name, trademark, manufacturer, or otherwise, does not necessarily constitute or imply its endorsement, recommendation, or favoring by the United States Government or the University of California. The views and opinions of authors expressed herein do not necessarily state or reflect those of the United States Government or the University of California, and shall not be used for advertising or product endorsement purposes.

Role of Interfacial Dislocations on Creep of a Fully Lamellar TiAl

T. G. Nieh and L. M. Hsiung

Lawrence Livermore National Laboratory, L-350, P.O. Box 808, Livermore, CA 94551, U.S.A.

Keywords: intermetallic alloy, creep, interface, interface sliding, deformation twinning, laminate, dislocation pileup,

Abstract

Deformation mechanisms of a fully lamellar TiAl (γ lamellae: 100 ~ 300 nm thick, α_2 lamellae: 10 ~ 50 nm thick) crept at 760°C have been investigated. It was found that, as a result of a fine structure, the motion and multiplication of dislocations within both γ and α_2 lamellae are limited at low creep stresses (< 400 MPa). Thus, the glide and climb of lattice dislocations have insignificant contribution to creep deformation. In contrast, the motion of interfacial dislocations on γ/α_2 and γ/γ interfaces (i.e. interface sliding) dominates the deformation at low stresses. The major obstacles impeding the motion of interfacial dislocations was found to be lattice dislocations impinging on lamellar interfaces. The number of impinging lattice dislocations increases as the applied stress increases and, subsequently, causes the pileup of interfacial dislocations on the interfaces. The pileup further leads to the formation of deformation twins. Deformation twinning activated by the pileup of interfacial dislocations is suggested to be the dominant deformation mechanism at high stresses (> 400 MPa).

Introduction

Two-phase [TiAl (γ)-Ti_3Al (α_2)] TiAl alloys have recently attracted more attention than single-phase γ-TiAl alloys because of their superior combination of room-temperature mechanical properties. Great efforts have been made to improve the creep resistance of two-phase TiAl alloys through alloy design and microstructural optimization. By controlling thermomechanical treatments, three different types of microstructures [equiaxed, duplex, and fully lamellar (*FL*)] have been developed [1]. It is well known that the creep resistance of two-phase alloys with a *FL* microstructure is better than that of the alloys with equiaxed and/or duplex microstructures [1-4]. Also, the creep resistance of powder metallurgy *FL*-TiAl alloys is superior to that of ingot metallurgy *FL*-TiAl alloys as a result of a refined lamellar microstructure [2]. Although a significant progress has been made in improving the creep resistance of TiAl alloys, little is known about the underlying creep mechanisms. Several studies on the creep behavior of *FL*-TiAl alloys have been made [3,5], only a few of the creep models have considered the contribution of interface sliding. The motion of interfacial dislocations was recently demonstrated to play an important role during the creep of *FL*-TiAl [6-8].

In a manner similar to other TiAl alloys, creep of fully lamellar *FL*-TiAl alloys revealed two distinct regimes, i.e. low stress (*LS*) and high stress (*HS*), as shown in Fig. 1 [8]. A nearly linear creep behavior was observed in the *LS* regime (< 400 MPa), i.e. $\dot{\varepsilon} = \kappa \cdot \sigma^n$ and n = 1.2 ~1.6, and a

power-law creep behavior with n = 6.7 ~ 10.1 in the *HS* regime (> 400 MPa.). An apparent activation energy Q of 160.4 kJ/mole was also obtained [8]. This value is much lower than the activation enthalpy (Q_v = 295 kJ/mole [9,10], 330 kJ/mole [11]) for lattice diffusion of Ti in γ-TiAl. However, it is close to the activation enthalpy for diffusion of O in γ-TiAl (177 kJ/mole) [12], O in Ti (168 kJ/mole) [13], O in Ti-6Al-4Zr-2Mo-2Sn (167.2 kJ/mole) [14], and C in Ti (127.6 kJ/mole) [15]. Also, the value is also close to the activation enthalpy for dislocation core diffusion ($Q_c/Q_v \approx 0.6$, i.e. 177 ~ 198 kJ/mole). This result indicates that the dislocation climb assisted by lattice diffusion within γ laths is probably not responsible for the creep deformation of refined *FL*-TiAl at low applied stresses. The purpose of the present investigation is to correlate creep behavior with deformation (interfacial) substructure to elucidate further the creep mechanisms of refined *FL*-TiAl.

Experimental

A *FL*-TiAl alloy with a nominal composition: Ti-47Al-2Cr-2Nb (in at. %) was used for this study. The alloy was fabricated by a hot-extrusion of gas-atomized titanium aluminide powder at 1400°C. The interstitial impurities [in parts per million (ppm) by weight] of the alloy are O: 780; N: 40; C: 260. Test specimens with a gauge dimension of 24.4 x 5.08 x 1.52 mm were prepared from the annealed alloy by electrical discharge machining. Creep tests were conducted in a dead-load creep machine with a lever arm ratio of 16:1. Tests were performed in air in a split furnace with three zones at 760°C. Detail information regarding the creep experiment and experimental data was reported elsewhere [2,8]. For current study, the deformation substructures of two tested specimens [one crept at a stress of 138 MPa (creep strain: ~0.25%) in the *LS* regime, and the other crept at a stress of 518 MPa (creep strain: ~3.6%) in the *HS* regime] were investigated. TEM foils were prepared by twin-jet electropolishing in a solution of 60 vol. % methanol, 35 vol. % butyl alcohol and 5 vol. % perchloric acid at ~15 V and –30°C. The microstructures of the crept alloys were examined using a JEOL-200CX transmission electron microscope equipped with a double-tilt goniometer stage. Images of dislocations were recorded using a weak–beam dark field (WBDF) imaging technique under *g (3g)* diffraction conditions.

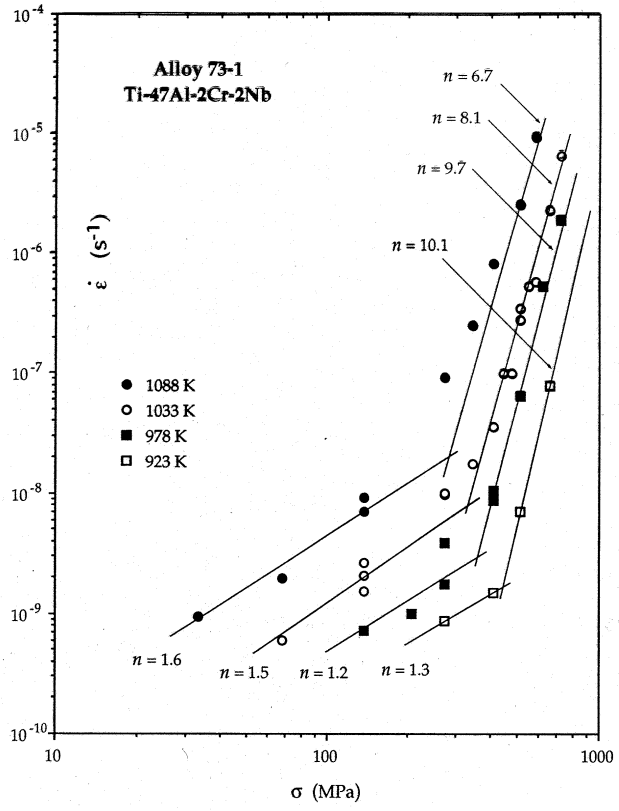

Fig. 1 Plots of steady state creep rates versus applied stress at testing temperatures between 650 and 815°C [8].

Results and discussion

Microstructure of As-Fabricated Alloy

A typical edge-on lamellar microstructure of the as-fabricated alloy is shown in Fig. 2 (left). The thicknesses of lamellae were measured to be in the range of 100 ~ 300 nm and 10 ~ 50 nm for γ and α_2, respectively. A WBDF image showing the dislocation substructure of the alloy is shown in Fig. 2 (right). Both lattice dislocations (*LD* hereafter), formed within γ lamellae, and interfacial dislocations (*ID* hereafter), formed on lamellar interfaces, can be readily seen. Evidently, the population of *ID* is much greater than that of *LD*. Here, *LD* includes both threading dislocation (i.e. dislocation terminates on the lamellar interfaces) and free dislocation (i.e. dislocation which is physically distant from the lamellar interfaces). It is noted that the density of threading dislocation is greater than that of free dislocation.

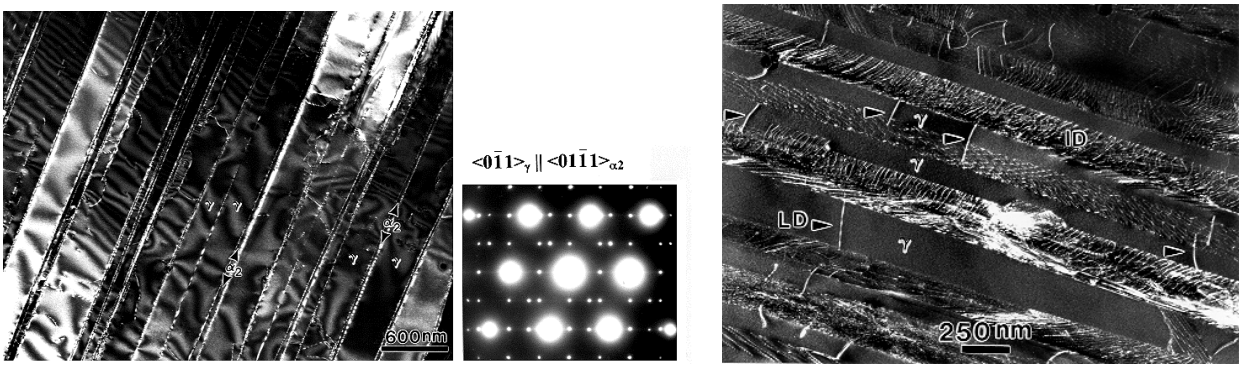

Fig. 2 Dark-field images showing typical dislocation substructures observed from an as-fabricated alloy sample; (left) edge-on view, and (right) tilt view.

Creep Deformation in the Low Stress (*LS*) regime

Deformation in a lamellar alloy is, in principle, caused by the multiplication and motion of *ID* and *LD*. Since α_2 is stronger than γ, and also the volume fraction of α_2 lamella is small (≤ 10%), deformation by the motion of *LD* is expected to occur mainly in the γ lamellae. Furthermore, due to the short moving distance of free dislocations the motion (bowing) of threading dislocations contributes primarily to deformation within the γ lamellae. In general, an applied shear stress must exceed the critical resolved shear stress in order to bow the threading dislocations. The critical resolved shear stress ($\tau_b \approx \mu b/d$) is dependent upon the thickness (d) of γ lamellae. Taking μ = 59 GPa (at 760°C), b = 0.28 nm, and d = 100 ~ 300 nm, the critical resolved shear stress is calculated to be τ_b = 55 ~ 165 MPa. Thus, the applied stress ($\sigma \approx 2\tau_b$) required to bow the threading dislocations is estimated to be greater than 110 ~ 330 MPa. Taking into account the fact that the motion and multiplication of *LD* in both γ and α_2 lamellae are limited in the *LS* regime, as a result of the refined lamellae, the motion of pre-existing *ID* is expected to become important to deformation. It is worth noting that the cooperative motion of *ID* in *FL*-TiAl deformed at room temperature has been observed previously in an *in situ* straining experiment [7]. We now present an indirect evidence of the motion of *ID* in FL-TiAl creep deformed at 760°C.

The interfacial substructure of a soft lamellar grain (oriented nearly ~45° with respect to the stress axis) in a sample crept at 138 MPa is shown in Fig. 3 (left). The appearance of fringe contrasts trailing along *ID* can be readily observed. The fringe contrasts can be best viewed when $2\pi \boldsymbol{g} \bullet \boldsymbol{R}$ = 2/3 or 4/3, where $\boldsymbol{g}$ is the reflection vector and $\boldsymbol{R}$ (= 1/3[111]) is the displacement vector of stacking fault in γ lamella; this suggests the formation of stacking faults on the wake of *ID*. The triangular features are presumably formed by the motion of three sets of *ID* arrays with Burgers

vectors: *1/6*[$\bar{1}\,\bar{1}\,2$], *1/6*[$1\,\bar{2}\,1$] and *1/6*[$\bar{2}\,11$]. The formation mechanism is schematically illustrated in Fig. 3 (right), where the equilibrium γ/α_2 interface resulted from both *ID* motion (pure shear) and chemical diffusion is lagging behind the non-equilibrium interface created solely by the motion of *ID*. Here, a stacking fault is formed as the first Shockley partial, *1/6*[$\bar{1}\,\bar{1}\,2$], glides along the interface, but is terminated by the glide of the second Shockley partial, 1/6[$1\bar{2}\,1$]. Then, another stacking fault is formed as the third Shockley partial, *1/6*[$\bar{2}\,11$], glides along.

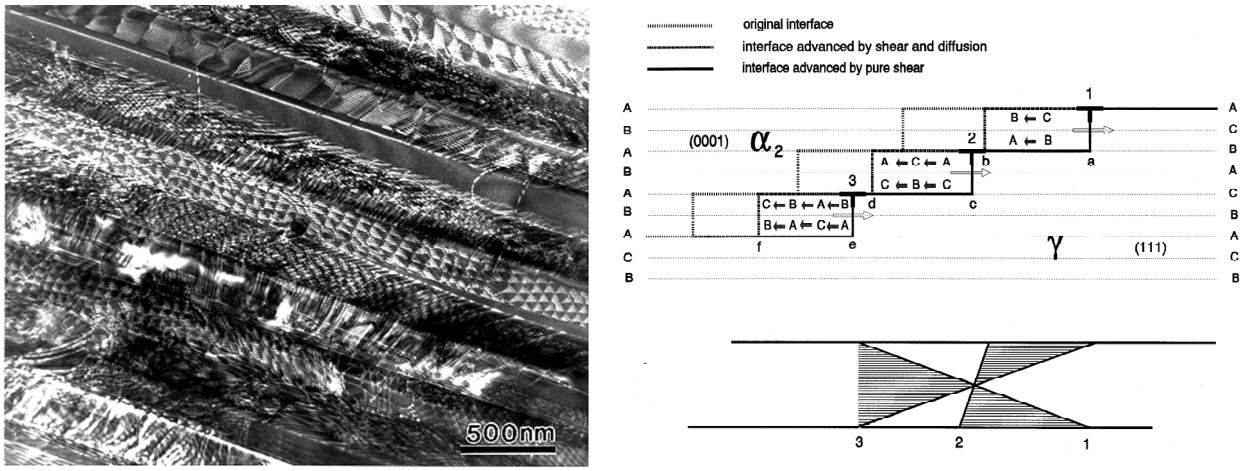

Fig. 3 (left) A WBDF image showing the appearance of fringe contrast trailing along *ID* on γ/α_2 and γ/γ interfaces, (right) a schematic illustration of the migration of γ/α_2 interface resulted from the cooperative motion of *ID* and chemical diffusion. Notice that the equilibrium interface is lagging behind the non-equilibrium interface generated by a pure shear. The triangular fault ribbons resulted from the motion of three different Shockley partials are also illustrated. The letters A, B and C stand for the stacking sequence.

It is noted that the highly populated *ID* and stacking faults on lamellar interfaces are expected to be the preferential sites for solute or impurity segregation. In fact, experimental evidence of solute segregation to γ/α_2 and γ/γ interfaces has recently been reported [16]. These solute segregants can act as short-range barriers for the motion of *ID,* in a manner similar to that of *Cottrell* atmosphere and *Suzuki* effect [17]; this results in the viscous glide of *ID*. The steady state creep rate may be described using the Orowan equation given below:

$$\dot{\varepsilon} = \Phi \rho_m b \bar{v} \qquad (1)$$

where Φ is a geometrical factor (for isotropic polycrystals: inverse of Taylor factor, for single crystal: Schmid factor), ρ_m is the density of mobile dislocations, b is the Burgers vector, and $\bar{v}$ is the average dislocation velocity. Since the multiplication of lattice dislocations within refined γ and α_2 lamellae is very limited when the material is deformed at low stress, the glide of pre-existing *ID* arrays becomes the predominant deformation mechanism. That is, the mobile dislocation density (ρ_m) is approximately equals to the density of *ID*. Under small creep-strain, low creep stress and strain-rate, it is plausible to assume that *ID* arrays are moving with a constant spacing so that the density of mobile dislocations is insensitive to the applied stress, i.e. $\rho_m \neq$ F (σ). Accordingly, the steady state creep rate ($\dot{\varepsilon}$) is mainly controlled by the average velocity ($\bar{v}$) of *ID* arrays [i.e. $\dot{\varepsilon}$ = F ($\bar{v}$)], which are considered to be drifting with the pinning solute (impurity) atoms at low applied stresses.

Let there be m solute atoms per unit length of dislocation line which effectively pin a dislocation line. When a unit length of *LD* drifts one atomic distance under an external stress σ, the estimated drift velocity of the dislocation line is of the order [17,18]:

$\bar{v} = (\sigma b^3 \nu/mkT) \exp(S/k) \exp(-Q/kT)$ (2)

where ν ($\sim 10^{12}$/sec) is the average vibration frequency of the dislocation line, S is the entropy of activation for the motion, and Q is the activation energy associated with the jump of a pinning atom. It is seen that the average dislocation velocity is linearly proportional to the applied stress. Consequently by combining Eqs. (1) and (2), a linear creep behavior [i.e. $\dot{\varepsilon} \propto \sigma^n \exp(-Q/kT)$, where n =1] is predicted provided all the mobile dislocations located on the interfaces are pinned by solute (impurity) atoms and no dislocation multiplication takes places. The slight deviation of n values from unity may be caused by dislocation multiplication on interface occurred as a result of dislocation pile-up [6,7], this event is expected to become more significant as creep strain and applied stress increase. For example, the stress due to a pile-up of n dislocations at a distance λ from the head of the pile-up is given approximately by [17,19]:

$\sigma = \mu n b/\pi\eta\lambda$ (3)

where $\eta = 1$ *or* $1-\nu$ for screw or edge dislocation, respectively. Since $n/\lambda \approx \rho_m$, thus

$\rho_m \approx \pi\eta\sigma/\mu b$ (4)

That is, when pile-up occurs, $\rho_m = f(\sigma)$, and the dislocation density proportionally increases with increasing shear stress. By inserting Eqs. (2) and (4) into Eq. (1), thus $\dot{\varepsilon} \propto \sigma^2 \exp(-Q/kT)$, i.e. n = 2 is obtained. Thus, the slight deviation of n from unity may be attributable to occurrence of local dislocation pile-up during the motion of interfacial dislocations at applied stresses < 400 MPa. In summary, the nearly linear relationship between strain rate and stress, and the fact that the activation energy is close to that for impurity or solute diffusion suggest that viscous glide of interfacial dislocations is the dominant deformation mechanism at low applied stresses.

Creep Deformation in the High Stress (*HS*) Regime

During the sliding of lamellar interfaces, the glide of *ID* is mainly impeded by impinged *LD*. A typical example is shown in Fig. 4. Here, a dislocation network formed by the reaction between impinged *LD* and intrinsic *ID* can be readily observed on a γ/α_2 Interface. Also noted is the mobility of *ID* suddenly decreases at site C and results in dislocation pileup. The occurrence of *LD* impingement on lamellar interfaces is expected to increase when the applied stress increases, i.e. more dislocation pileups would be formed at higher applied stresses.

Deformation twinning was found to be an important deformation mechanism when the alloy was creep deformed at stresses greater than 400 MPa. An example is given in Fig. 5 (left). Here, the $(\bar{1}11)$ [211]-type deformation twins (*DT* hereafter) formed within γ lamellae in a specimen crept at 518 MPa. It is noted that one of the twin lamellae was still growing between two lamellar interfaces, and its growth would be eventually terminated by the lower interface. This observation suggests that lamellar interfaces are preferred nucleation sites for *DT*, presumably resulting from the high local stresses caused by the pileup of *ID*. That is, deformation twinning in *FL*-TiAl is a result of stress relaxation along the interfaces [6,20,21].

The stress concentration (τ_e) at the tip of the pileup of n dislocations can be estimated by $\tau_e = n\tau_i$, where τ_i is the resolved shear stress acting on the lamellar interface. To relieve the stress concentration, the $(\bar{1}11)$-type twins are nucleated from the interface by successive dissociation reaction of *ID*: $1/6[\bar{1}2\bar{1}]_{(111)} \rightarrow 1/6[011]_{(100)} + 1/6[\bar{1}1\bar{2}]_{(\bar{1}11)}$. This dislocation reaction for twinning is schematically illustrated in Fig. 5 (right), where $1/6[1\bar{1}2]$ is the twinning dislocation on $(\bar{1}11)$ plane and $1/6[011]$ is the stair-rod (residual) dislocation on (100) plane. It is anticipated that the dislocation reaction $1/6[\bar{1}1\bar{2}]_{(\bar{1}11)} + 1/6[1\bar{2}1]_{(111)} \rightarrow 1/6[0\bar{1}\bar{1}]_{(100)}$ could also take place when the twin lamella impinges onto the lamellar interface. This reaction again results in the formation

of *1/6*[$0\bar{1}\bar{1}$] stair-rod dislocations on the interface. The formation of stair-rod dislocations at the junctions between *DT* and lamellar interface is demonstrated in Fig. 6, where the array of *1/6*[011] stair-rod dislocations becomes invisible [Fig. 6 (left)] and/or visible [Fig. 6 (right)] when the reflection vectors (***g***) of *200* and/or *012* are used for imaging. Note that the stair-rod dislocations can not be resolved individually because of an extremely short distance (0.25 nm) between stair-rod dislocations.

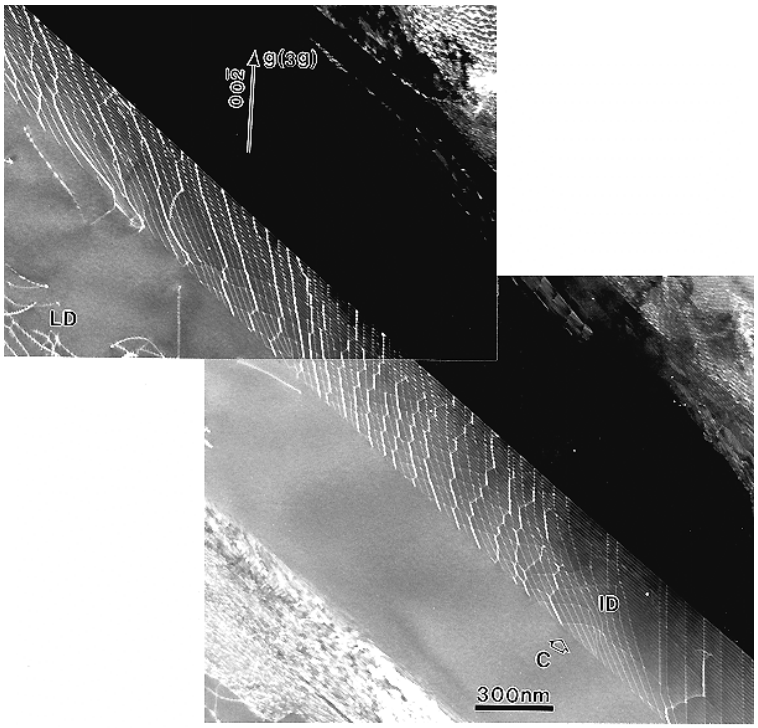

Fig. 4 A WBDF image showing that the motion of interfacial dislocations is impeded as a result of the formation of dislocation nodes (junctions) due to the reaction between impinged *LD* (stronger contrast) and intrinsic *ID* (weaker contrast).

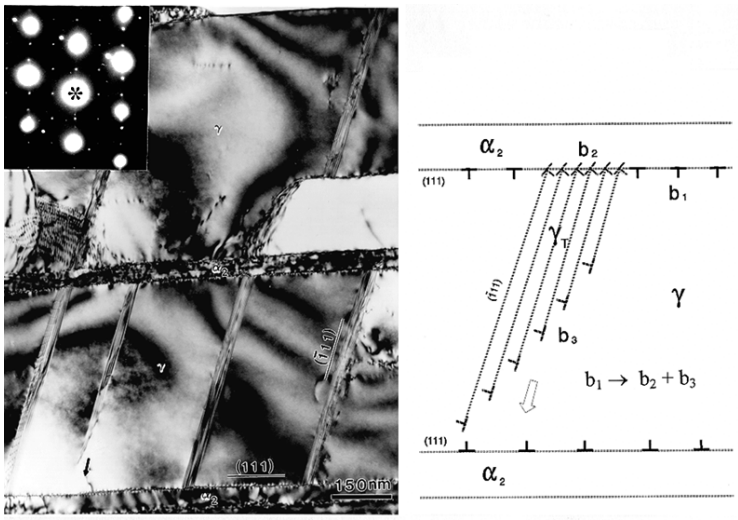

Fig. 5 (Left) A bright-field TEM image showing several ($\bar{1}11$) type *DT* formed within γ lamellae. Notice that one of the twin lamellae was growing between two lamellar interfaces (marked by an

arrow). (Right) Schematic illustration of the nucleation of a $(\bar{1}11)$ type *DT* from a γ/α_2 interface, where b_1, b_2, and b_3 denote the interfacial, stair-rod, and twinning dislocations, respectively.

Based on the above observations, it is proposed that the twinning process activated by the pileup of *ID* is the dominant creep mechanism in the *HS* regime. In this case, the creep rate ($\dot{\varepsilon}$) may be, in principle, expressed by

$$\dot{\varepsilon} = M\,(\dot{N}\bullet\Delta t)\,L\,b\,\bar{v} \qquad (5)$$

where, M is the number of twin sources per unit volume, $(\dot{N}\bullet\Delta t)$ is the number of twinning dislocations emitted from a twin source, L is the length of twinning dislocation, b is the length of Burgers vector, and $\bar{v}$ is the average velocity of twinning dislocation. Quantitatively, $M, \dot{N}$, and $\bar{v}$ in the equation are dependent upon the applied stress and initial microstructure. A rigorous quantitative creep model based upon the twinning process is currently underway.

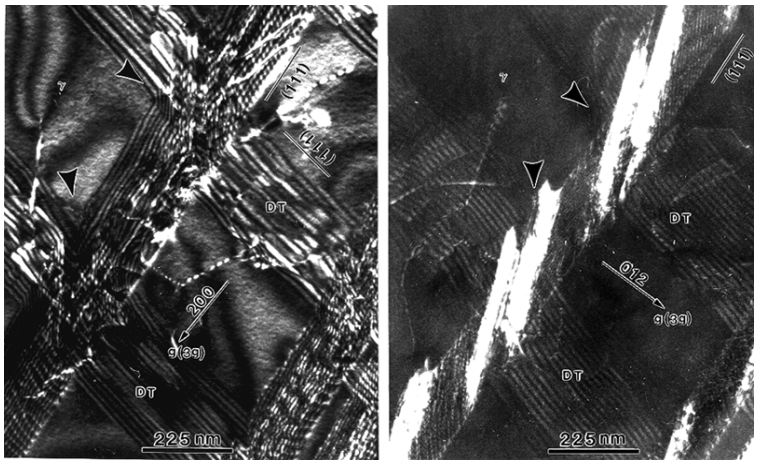

Fig. 6 Paired WBDF images showing the existence of *1/6*[011] stair-rod dislocations at the intersections (indicated by arrows) between the $(\bar{1}11)$ type *DT* and a α_2 lamella. (Left) Invisible at ***g*** = *200 (****g*****•*****b*** = *0)*, (right) visible at ***g*** = *021*, **Z** (zone axis) ≈ $[0\bar{1}2]$.

Summary

Creep mechanisms of *FL*-TiAl with a refined lamellar microstructure (γ lamellae: 100 ~ 300 nm thick, α_2 lamellae: 10 ~ 50 nm thick) have been investigated. In the low stress regime (< 400 MPa). the motion and multiplication of lattice dislocations are limited because the refined lamellar spacing, a cooperative motion of interfacial dislocations (i.e. interface sliding) is proposed to be the dominant deformation mechanism. During the sliding of lamellar interfaces, the motion of interfacial dislocations is interrupted by the impinged lattice dislocations on the interfaces and results in the pileup of interfacial dislocations. This is a prevalent process especially at high stresses. To relieve stress concentration at the head of dislocation pileup, $(\bar{1}11)$-type deformation twins are observed to emit from the interfaces through the dissociation reaction of interfacial dislocations: $1/6[\bar{1}2\bar{1}]_{(111)} \rightarrow 1/6[011]_{(100)} + 1/6[\bar{1}1\bar{2}]_{(\bar{1}11)}$. It is thus suggested that deformation twinning activated by the pileup of interfacial dislocations is the dominant deformation mechanism in the high stress regime (> 400 MPa).

Acknowledgment

This work was performed under the auspices of the U.S. Department of Energy by Lawrence Livermore National Laboratory under contract No. W–7405–Eng–48.

References

1. Y –W. Kim, *Acta Metall. Mater*. **40**, 1121 (1992).
2. J. N. Wang, A. J. Schwartz, T. G. Nieh, C. T. Liu, V. K. Sikka and D. R. Clemens, in *Gamma Titanium Aluminides*, ed. Y-W. Kim et al., TMS (1995), p. 949.
3. J. Beddoes, W. Wallace and L. Zhao, *Intr. Mater. Rev*., **40**, 97 (1995).
4. C. T. Liu, P. J. Maziasz and J. L. Wright, *Mat. Res. Soc. Symp. Proc*., **460**, 83 (1997).
5. T. A. Parthasarathy, M.G. Mendiratta and D.M. Dimiduk, *Scripta Mater.*, **37**, 315 (1997).
6. L. M. Hsiung and T. G. Nieh, *Mater. Sci. Engrg*., **A239-240**, 438 (1997).
7. L. M. Hsiung, A. J. Schwartz and T. G. Nieh, *Scripta Mater*. **36**, 1017 (1997).
8. J. N. Wang and T. G. Nieh, *Acta Mater*., **46**, 1887 (1998).
9. H. Mehrer, W. Sprengel and M. Denkinger, in *Diffusion in Ordered alloys*, Eds. B. Fulta et al., TMS (1993), p. 51.
10. W. Sprengel, N. Oikawa, H. Nakajima, *Intermetallics*, **4**, 185 (1996).
11. H. Oikawa, in *High Temperature Aluminides and Intermetallics*, Eds. S. H. Whang et al., TMS (1989), p. 353.
12. Y. A. Chang, R. Kieschke, J. DeKock and M. X. Zhang, in *Control of Interfaces in Metal and Ceramics Composites*, edited by R. Y. Lin and S. G. Fishman, TMS (1993), p. 3.
13. C. R. Brooks, in *Metals Handbook* (Desk Edition, 1985), edited by H. E. Boyer and T. L. Gall, ASM (Metals Park, OH), 28•66(T).
14. R. N. Shenoy, J. Unnam and R. K. Clark, in *Oxidation of Metals*, **26**, 105 (1986).
15. A. I., Nakonechnikov and L. V. Parlinov, *Diffusion Data*, **6**, 573 (1972).
16. C. T. Liu, P. J. Maziasz, and D. J. Larson, in *Interstitial and Substitutional Solute Effects in Intermetallics*, Eds. Baker et al., TMS (1998), p. 179.
17. J. Weertman and J. R. Weertman, *Elementary Dislocation Theory*, Macmillan, NewYork (1964).
18. J. P. Hirth and J. Lothe, *Theory of Dislocations*, McGraw-Hill, New York (1968).
19. J. D. Eshelby, F. C. Frank and F. R. N. Nabarro, *Phil. Mag*. **42**, 351 (1951).
20. T. Mori and H. Fujita, *Acta Metall*., **28**, 771 (1980).
21. M. H. Yoo, *Scripta Mater*., **39**, 569 (1998).